chemosensors

MDPI

Article

Highly Dispersive Palladium Loading on ZnO by Galvanic Replacements with Improved Methane Sensing Performance

Renjie Chen [1,†], Shirui Luo [1,†], Dan Xie [2], Yangxin Yu [3] and Lan Xiang [1,*]

1 Department of Chemical Engineering, Tsinghua University, Beijing 100084, China
2 School of Integrated Circuits, Tsinghua University, Beijing 100084, China
3 Lab of Chemical Engineering Thermodynamics, Department of Chemical Engineering, Tsinghua University, Beijing 100084, China
* Correspondence: xianglan@mail.tsinghua.edu.cn
† These authors contributed equally to this work.

Abstract: Methane detection is important for the safety of production and life. Metal oxide semiconductor (MOS) methane detection is a mature and widely used technology but still experiences problems such as unsatisfying low-temperature sensing performances. In this study, ZnO/Pd with Pd nanoparticles of different diameters was prepared to study the influence of Pd dispersion on CH_4 sensing properties. Results showed that CH_4 sensing enhancements were positively correlated with the dispersity of Pd. Moreover, by galvanic replacement using Ag as the sacrificial template, a highly dispersive loading of Pd on ZnO was realized, and the CH_4 sensing performance was further enhanced while the amount of Pd reduced from 1.35 wt% to 0.26 wt%. Experiments and DFT calculation indicated that improved CH_4 sensing performance resulted from abundant catalytic sites induced by highly dispersed Pd NPs and the enhanced CH_4 adsorption on positively charged Pds caused by electrons transferred from Pd to Ag. This study provides a strategy to achieve high dispersion of Pd to maximize the utilization of noble metal, which is promising for lowering the cost of the MOS-based CH_4 sensors.

Keywords: methane sensing; ZnO; Pd; galvanic replacement; density functional theory(DFT)

Citation: Chen, R.; Luo, S.; Xie, D.; Yu, Y.; Xiang, L. Highly Dispersive Palladium Loading on ZnO by Galvanic Replacements with Improved Methane Sensing Performance. *Chemosensors* **2022**, *10*, 329. https://doi.org/10.3390/chemosensors10080329

Academic Editor: Andrea Ponzoni

Received: 26 July 2022
Accepted: 11 August 2022
Published: 12 August 2022

1. Introduction

Methane is a flammable and explosive gas with an explosion limit of 5–15% at room temperature [1], which has potential safety hazards. Therefore, the real-time and rapid detection of methane is the key to minimizing the loss of life and property. Catalytic combustion type sensors are widely used for methane detection in coal mines at this stage due to their simplicity, low cost, and fast detection. However, their high operating temperature (600–800 °C) consumes a high amount of energy and leads to a short lifetime due to the catalyst's degradation [2–4]. Metal oxide semiconductor (MOS) based gas sensors are promising for methane detection due to their relatively low operating temperatures (200–500 °C), the ease of fabrication and low costs [5–8], such as SnO_2 [9], ZnO [10], TiO_2 [11] and WO_3 [12]. To further reduce energy consumption, there is still room to reduce the operating temperature of MOS gas sensors. Previous studies have shown that loading noble metals (Pd, Pt, Au, Ag, etc.) on the surface of metal oxides is beneficial for lowering the operating temperature due to their excellent catalytic properties that promote methane dissociation and reduce the activation energy of methane oxidation [13–16]. Among the noble metals, Pd is the most concentrated for its promotion to C-H bond cleavage and shows the best performance in CH_4 sensing.

However, the current utilization of Pd on the surface of MOS is usually low due to their relatively large size, which means that only the surface atoms is functional while the bulk atoms are not employed. One of the effective methods for improving the utilization is to reduce the size of Pd nanoparticles (NPs). Luo et al. realized highly dispersed Pd

NPs with diameters of 2–5 nm taking advantage of the confinement of ZIF-8 cavity, which limited the growth of Pd NPs [17]. Sun et al. synthesized highly dispersed Pd NPs with diameters of 3–6 nm by introducing positive potential sites such as an SBA-15 molecular sieve on the surface of CeO_2, which generates strong electrostatic adsorption with the anion $PdCl_4^{2-}$. Therefore the size of Pd is limited by the size of positive potential sites [18]. Nevertheless, the methods that introduce extra substances usually isolated the contact of MOS with Pd, and the sensing enhancement of Pd is not functional. In addition, the introduction of other substances would also affect CH_4 diffusion.

To better improve the Pd utilization in the MOS CH_4 sensing system, galvanic replacement (GR) is a promising method [19,20]. The galvanic replacement reaction is a thermodynamically spontaneous redox process driven by the standard electrode potentials difference of the two metals. The method requires a second metal as the sacrificial template, on which Pd is highly dispersed through GR reaction [21,22]. Usually Ag (+0.799 V vs. SHE) is considered as the most suitable choice for Pd (+0.915 V vs. SHE). Moreover, the price of Ag is approximately 1/100 of Pd. Therefore, the cost of the MOS-based CH_4 sensor could be significantly decreased by using the GR method.

In this study, ZnO/Pd material with controlled diameters of Pd NPs was prepared firstly to investigate the influence of the amount and dispersion of Pd on the CH_4 sensing properties. Then, in order to further improve the dispersion of Pd on ZnO, the GR method is applied using Ag as the sacrificial template to synthesize the ZnO/Ag@Pd. The Pd dispersion is remarkably improved by galvanic replacements with enhanced CH_4 sensing performances, and the amount of Pd greatly reduced to 0.23 wt% compared with ZnO/Pd (1.37 wt%). Finally, the synergistic effect of Ag@Pd in CH_4 sensing is investigated by density functional theory calculations.

2. Materials and Methods

2.1. Synthesis

For the preparation of ZnO nanorod, 1.756 g $ZnAc_2$ and 0.200 g polyvinylpyrrolidone (PVP) were added into 200 mL of ethanol, and 8.000 g NaOH was added into 200 mL of ethanol. Both solutions were heated and stirred at 60 °C to fully dissolve them in order to prepare the $ZnAc_2$ alcohol solution and the NaOH alcohol solution. After cooling to room temperature, the $ZnAc_2$ alcohol solution was added dropwise to the NaOH alcohol solution at a constant rate of 5.85 mL/min using a peristaltic pump by thoroughly stirring throughout this procedure. After complete dropwise addition, the solution was centrifuged, the supernatant was discarded, and the precipitate was used as ZnO seeds.

ZnO nanorods as the starting materials were synthesized using ε-$Zn(OH)_2$ as the precursor [23]. The precursor solution was obtained by dissolving 1.2 g ε-$Zn(OH)_2$ in 40 mL of 2 M NaOH solution and stirring at room temperature for 20 min to form a suspension. The suspension was repeatedly flushed with a dropper to mix with the pre-prepared ZnO seeds and the suspension was heated and stirred for 30 min at 80 °C. The precipitate was filtered, washed and dried to obtain ZnO nanorods.

For the preparation of ZnO/Pd, 0.4 g of ZnO nanorods, 0.01 g of $PdCl_2$ and a certain amount of PVP were dispersed into 80 mL of ethylene glycol to form a suspension. Then the suspension was heated at 100 °C for 3 h. Finally, the precipitate was washed and dried at 60 °C overnight, and ZnO/Pd was obtained.

For the preparation of ZnO/Ag, 0.1 g of ZnO nanorods, 0.01 g of $AgNO_3$ and 0.10 g PVP were dispersed into 20 mL of ethylene glycol to form a suspension. Then the suspension was heated at 50 °C for 1 h. Finally, the precipitate was washed and dried at 60 °C overnight, and ZnO/Ag was obtained.

ZnO/Ag@Pd was prepared by a facile galvanic replacement method. Firstly, 0.01 g $PdCl_2$ was dissolved into 10 mL 0.04 M hydrochloric acid to prepare a $PdCl_2$ solution. Then, 0.05 g of ZnO/Ag composite and 1 mL of $PdCl_2$ solution were added into 20 mL of deionized water, and then the mixture was kept for 30 min at room temperature. The

precipitate was washed and dried at 60 °C overnight, and then the ZnO/Ag@Pd composite was obtained.

2.2. Characterization

The morphology and microstructure of the samples were examined by field emission scanning electron microscopy (FESEM, JSM 7401F, JEOL, Tokyo, Japan) and high-resolution transmission electron microscopy ((HRTEM, JEM-2010, JEOL, Tokyo, Japan), respectively. The surface composition of the samples was characterized by X-ray photoelectron spectrometry (XPS, PHI-5300, PHI, Chanhassen, USA). Powder X-ray diffraction (XRD) analysis was performed using an X-ray diffractometer (D8 Advance, Bruker, Karlsruhe, Germany) with Cu Kα (λ = 0.154178 nm) radiation for phase identification. An inductively coupled plasma (ICP) spectrometer (Thermo IRIS Intrepid II type) was used to detect the content of specific elements in the samples. A series of standard solutions with a concentration gradient was prepared, and the sample to be tested was dissolved with acid. Temperature-programmed desorption (TPD) of adsorbed oxygen was carried out using Quantachrome ChemBET Pulsar TPR/TPD. In a typical CO-TPD measurement, the sample was initially treated with He at 200 °C for 30 min and then cooled down to 90 °C. Afterwards, the sample was exposed to a mixture of CO and He at 90 °C for 45 min. Then the sample was cooled down to 50 °C and flushed with He. CO-TPD analysis was performed with a heating rate of 10 K min^{-1} up to 600 °C.

2.3. Gas Sensor Fabrication and Gas Sensing Tests

The sample to be tested was grinded thoroughly with deionized water with a concentration of 3.0 g/L to form a slurry. A small amount of the grinded slurry was dipped with a brush and applied evenly on the alumina ceramic tube. The ceramic tube was heated at 250 °C for 3 h to stabilize the powdered composite material bonded to the alumina surface. Using an AS-20 sensor aging table (Beijing Elite Tech. Co., Ltd., Beijing, China), the ceramic tube was aged for 24 h at 160 mA to stabilize its sensing performance. [24] The resistance of the tube was measured by the CGS-8 Intelligent Gas Sensing Analysis System (Beijing Elite Tech. Co., Ltd., Beijing, China). The target concentration of methane (500 ppm–10,000 ppm) was obtained by the injection of certain volume of methane into the fixed chamber with a volume of 20 L, and the variation of the sensor resistance over time was obtained from the analysis system. The response of the sensor is defined as $(R_a - R_g)/R_g \times 100$ (%), where R_a and R_g are the film resistance in air and methane, respectively.

2.4. Computational Methodology

Density function theory (DFT) calculations were performed by the $Dmol^3$ program [25,26] in Materials Studio, using the Spin Restricted method. All calculations were performed using the Perdew–Burke–Ernzerhof (PBE) generalized gradient approximation (GGA) [27] for the description of the atomic orbitals. The electron truncation energy was taken as 500 eV.

In calculating the structure of the metal surface, the cell model is a 3-layer infinitely extended plane, using a 3 × 3 supercell structure for calculations with a metal surface vacuum layer thickness of 15 Å. Fixing the lower atomic coordinates, the relaxation is performed on the surface atoms. The Brillouin zone is sampled at k points using a 4 × 4 × 1 grid with a grid length of 0.025 $Å^{-1}$ as the basis for inverse easy space integration.

For the calculations using the DFT method, all possible adsorption sites were selected for the adsorption energy calculations involved, and the adsorption site with the largest adsorption energy was taken as the most stable adsorption site. The adsorption energy calculation is calculated as follows:

$$E_{abs} = E_{composite} - E_{CH_4} - E_{metal}$$

where E_{abs} represents the adsorption energy; $E_{composite}$ represents the energy of a single gas molecule adsorbed on the blank metal surface to form a composite structure; E_{CH_4} represents the energy of a single CH_4 molecule; and E_{metal} represents the energy of the blank metal surface.

3. Results and Discussion

3.1. Effect of Pd Dispersion on the CH_4 Sensing Performance

ZnO/Pd with Pd NPs of different diameter was firstly synthesized to investigate the effect of Pd dispersion on CH_4 sensing performance by adjusting the amount of PVP during the preparation of ZnO/Pd materials (0 g, 0.02 g, 0.05 g, and 0.10 g), and the four samples were labelled as ZnO/Pd-0, 1, 2 and 3. As observed in the SEM images of Figure 1b, the ZnO/Pd material, starting from a center, radially grows many ZnO nanorods in a spiky spherical structure in all directions. The average radius of an individual nanorod is ~15 nm, and the length of nanorod is 0.5–2 μm. From the XRD diffraction pattern of Figure 1a, the peaks at 31.77°, 34.42°, and 36.35° correspond to ZnO(100), (001), and (101) crystalline planes (PCPDF 36-1451), respectively, while the peak at 40.20° corresponds to the Pd(111) crystalline plane (PCPDF 89-4897). As the amount of PVP increases, the peak of Pd(111) becomes wider and lower, indicating that the size of Pd NPs becomes smaller. The HRTEM image in Figure 1c of ZnO/Pd-2 shows the crystalline spacing of 0.522 nm and 0.224 nm, which corresponds to ZnO(001) and Pd(111) crystalline planes, respectively, and showed great correspondence with XRD results.

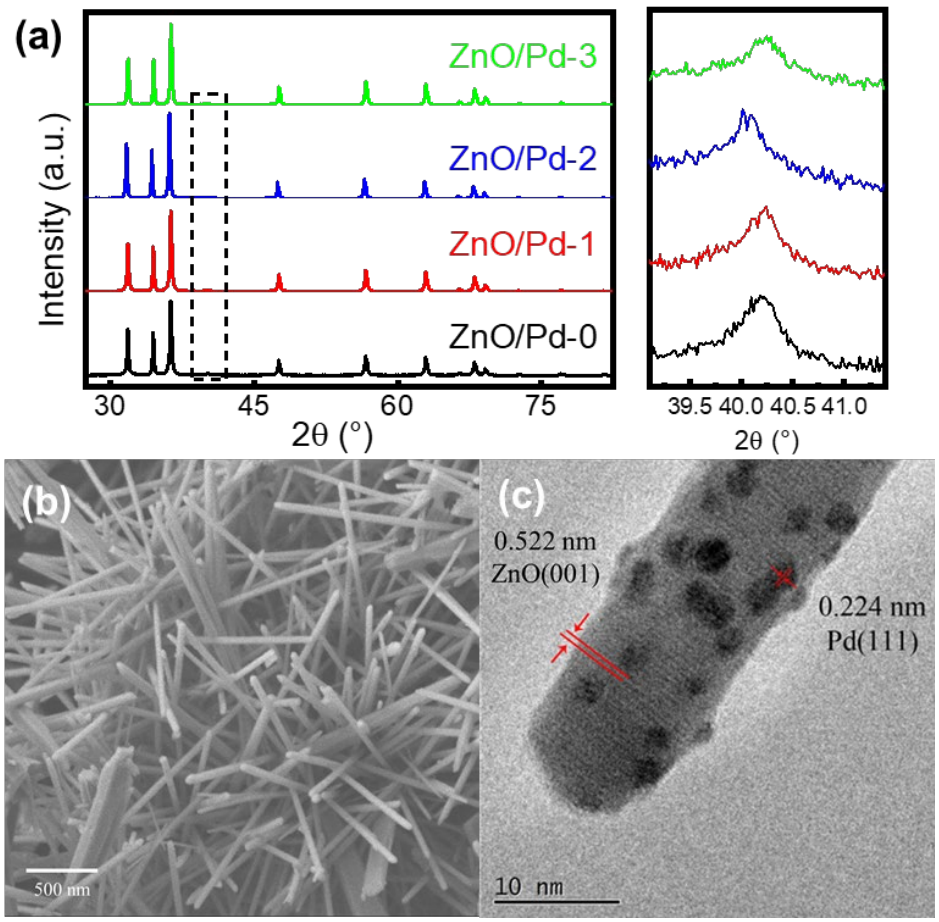

Figure 1. (**a**) XRD patterns of ZnO/Pd-0, 1, 2 and 3. (**b**) SEM and (**c**) TEM image of ZnO/Pd-2.

It can be observed from Figure 2 that the average particle size of Pd NPs was 8.63, 5.78, 2.67, and 2.54 nm for ZnO/Pd-0, 1, 2, and 3, respectively, since PVP limits the growth and

agglomeration of metal NPs due to its capping effect [28]. Pd NPs are uniformly loaded on ZnO nanorods. However, there is no significant difference between the size of Pd NPs in ZnO/Pd-2 and ZnO/Pd-3, indicating that the size of Pd NPs cannot be further reduced by increasing the amount of PVP.

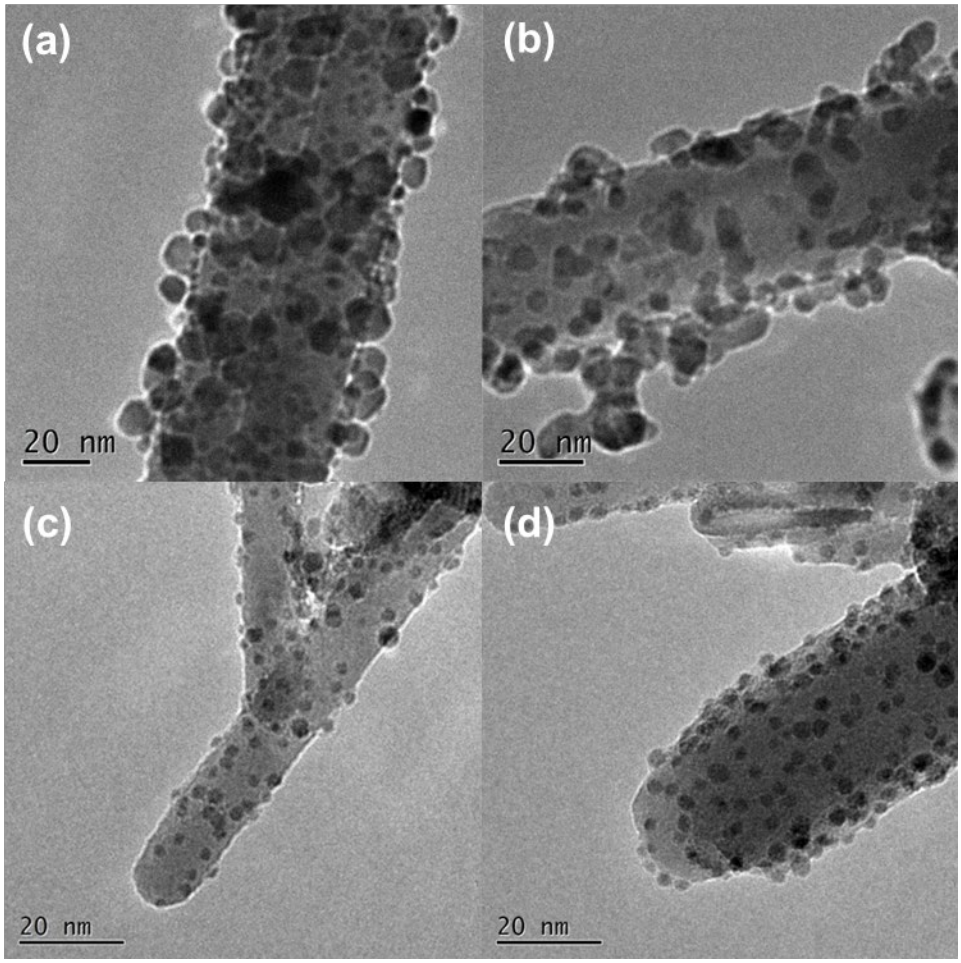

Figure 2. TEM images of (**a**) ZnO/Pd-0, (**b**) ZnO/Pd-1, (**c**) ZnO/Pd-2 and (**d**) ZnO/Pd-3.

The sensing properties of ZnO and four ZnO/Pd samples to 500 ppm CH_4 at different temperatures were tested, and the response results are summarized in Figure 3. Compared with ZnO, four ZnO/Pd samples all showed improved CH_4 sensing performance with decreased optimal temperatures (280 °C to 230 °C) and increased responses, indicating the catalytic promotion by Pd. The CH_4 response increased as the size of Pd NPs decreased, and ZnO/Pd-2 and ZnO/Pd-3 show the highest CH_4 response at about 27%. Thus, it can be concluded that CH_4 responses have a negative correlation to the size of Pd NPs; i.e., it is positively correlated with the dispersity of Pd. The smaller the particle size of Pd NPs, the better the dispersity of Pd, and the higher the response value of ZnO/Pd relative to CH_4. Pd contents in four ZnO/Pd materials were analyzed using ICP. It was found that Pd contents were 3.26%, 2.49%, 1.35% and 1.41 wt% for ZnO/Pd-0, 1, 2, and 3, respectively. Combined with TEM observations, both the size and the amount of Pd cannot be further reduced by adding more PVP.

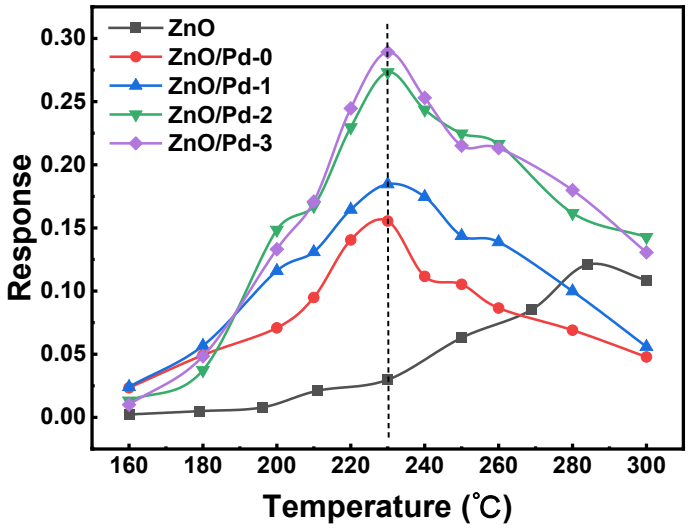

Figure 3. Response of ZnO, ZnO/Pd-0, 1, 2 and 3 to 500 ppm CH_4 at different temperatures.

3.2. Highly Dispersive Pd with Enhanced CH_4 Sensing Performance via Galvanic Replacement

In order to further reduce the size and the amount of Pd, (i.e., improving dispersity), the GR method was deployed using Ag as a sacrificial template. The reaction of Pd^{2+} with Ag NPs on the ZnO surface occurs as follows: $Pd^{2+} + 2Ag \rightarrow Pd + 2Ag^{+}$. The schematic diagram is shown in Figure 4a.

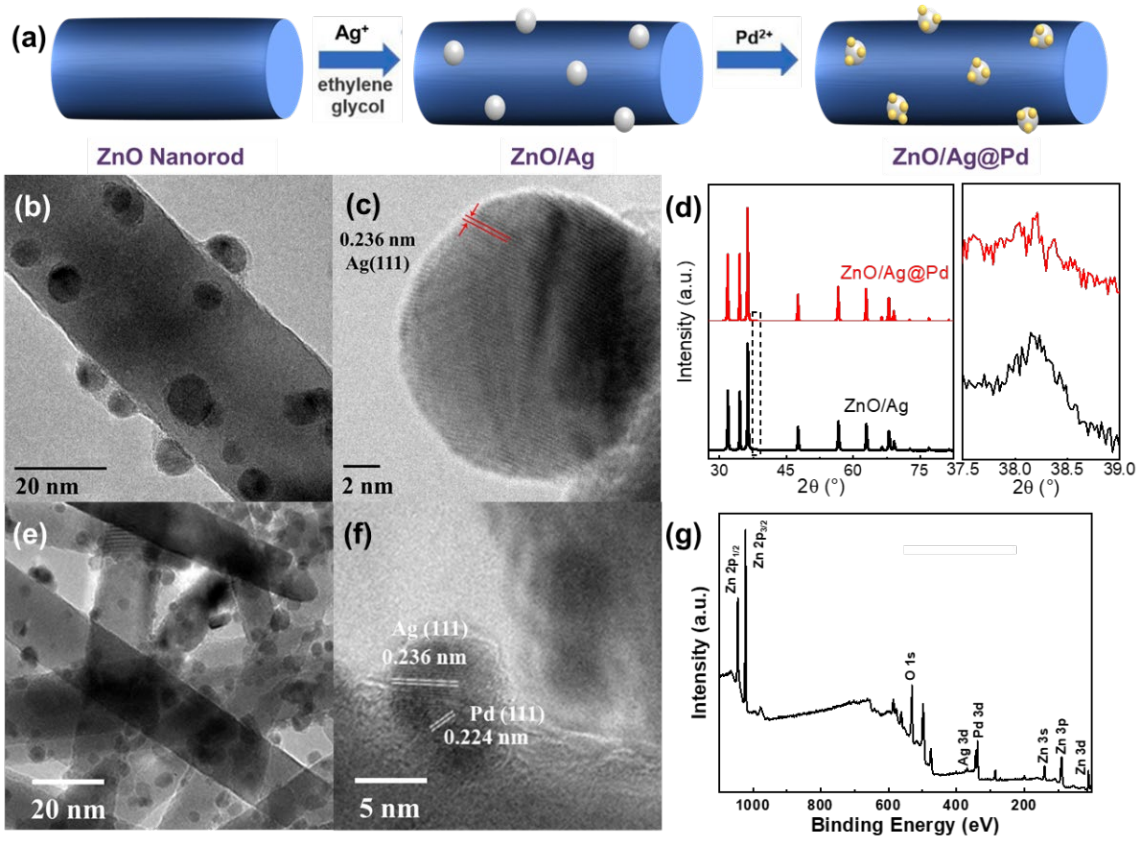

Figure 4. (**a**) Schematic illustration for the fabrication of ZnO/Ag@Pd. (**b**,**c**) TEM image of ZnO/Ag. (**d**) XRD patterns of ZnO/Ag and ZnO/Ag@Pd. (**e**,**f**) TEM image of ZnO/Ag@Pd. (**g**) Overall XPS spectra of ZnO/Ag@Pd.

As shown in Figure 4b, Ag NPs with an average diameter of 8 nm are uniformly loaded on ZnO nanorods. After GR reaction, the ZnO/Ag@Pd was prepared. From the XRD diffraction pattern of Figure 4d, the peak at 38.12° can be indexed to the Ag(111) crystal plane (PCPDF 89-3722), which is consistent with the HRTEM image with a crystalline spacing of 0.236 nm in Figure 4c. Figure 4f shows that the crystal plane spacing of the particles on ZnO/Ag@Pd is 0.224 nm and 0.236 nm, which should be identified as the Pd(111) and Ag(111) crystal plane spacing, respectively. Compared with the ZnO/Pd (all ZnO/Pd in the following refers to ZnO/Pd-2), Pd NPs on ZnO/Ag@Pd are denser and more uniform, and the particle size is significantly reduced from 2–4 nm to 1–2 nm. From the XRD patterns of ZnO/Ag@Pd in Figure 4d, the Ag(111) peak could not be indexed as the Ag had been sacrificed, and the Pd(111) peak was also absent due to its ultra-small size. The overall XPS spectrum in Figure 4g confirms the coexistence of Ag and Pd. Moreover, by comparing the fine-scanned XPS spectrum of Pd and Ag in ZnO/Pd, ZnO/Ag, and ZnO/Ag@Pd in Figure 5, the $3d_{3/2}$ and $3d_{5/2}$ peaks of Pd shifted from 340.1, 334.9 eV to a higher level of 342.3 and 337.1 eV, while the $3d_{3/2}$ and $3d_{5/2}$ peak of Ag shifted from 373.5 and 367.5 eV to lower levels at 367.5 and 367.1 eV, respectively, indicating that Pd and Ag form an alloy in the ZnO/Ag@Pd with electrons transferring from Pd to Ag. According to ICP results, the Pd content in ZnO/Ag@Pd significantly decreased from 1.35 wt% (ZnO/Pd) to 0.23 wt%. The above results indicated that highly dispersive Pd was successfully achieved by using the GR method.

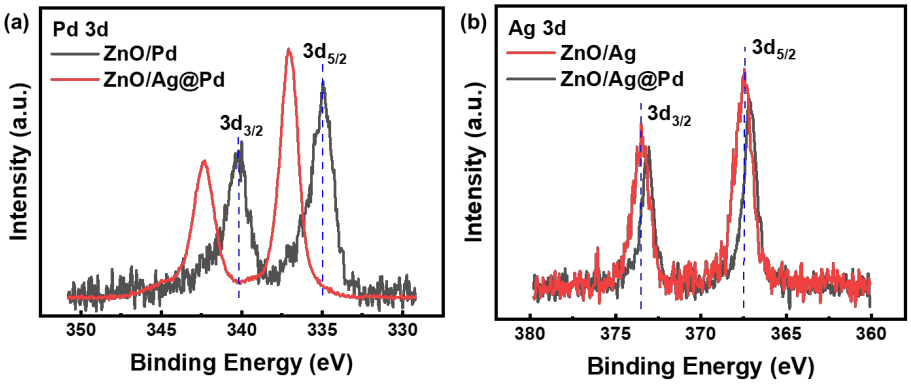

Figure 5. (**a**) Fine-scanned Pd 3d XPS spectras of ZnO/Pd and ZnO/Ag@Pd. (**b**) Fine-scanned Ag 3d XPS spectras of ZnO/Ag and ZnO/Ag@Pd.

The responses of ZnO/Pd, ZnO/Ag, and ZnO/Ag@Pd to 500 ppm CH_4 at 160–280 °C were tested, and the results are shown in Figure 6a. The response value of ZnO/Ag is much weaker than ZnO/Pd and the CH_4 response become significant at temperatures higher than 260 °C, while the response of ZnO/Ag@Pd is higher than that of ZnO/Pd at all temperature ranges. The dynamic response curves of three samples at 230 °C are shown in Figure 6b, as all samples show fast responses to CH_4, with response/recovery times less than 10 s, and ZnO/Ag@Pd showed the highest response of 32.6%. However, the optimal temperature of ZnO/Ag@Pd was higher than that of ZnO/Pd, and the corresponding response-temperature behavior was more similar to that of ZnO/Ag, which means that Pd can work as the sensing promoter to ZnO/Ag. From the above results, it can be concluded that the GR method using Ag as sacrificial metals can significantly improve the dispersity of Pd and reduce the amount of Pd at the same time. The highly dispersive Pd can provide more active sites for C-H cleavage, and, therefore, accelerate CH_4 oxidation to achieve improved CH_4 sensing performance.

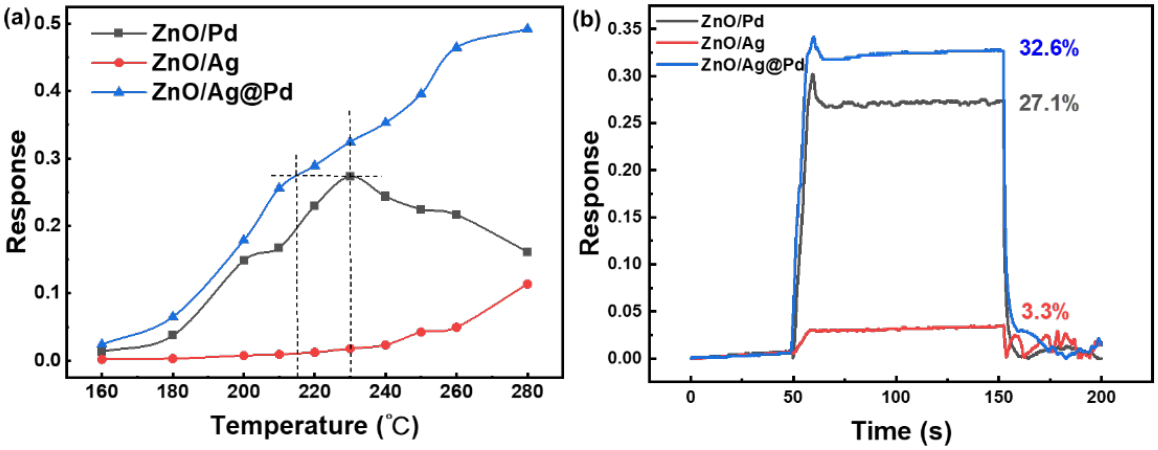

Figure 6. (**a**) Response to 500 ppm CH_4 of ZnO/Pd, ZnO/Ag and ZnO/Ag@Pd at different temperatures. (**b**) Dynamic response curves of ZnO/Pd, ZnO/Ag and ZnO/Ag@Pd to 500 ppm CH_4 at 230 °C.

3.3. Mechanism

To further investigate the mechanism, ZnO/Pd, ZnO/Ag, and ZnO/Ag@Pd materials were analyzed by conducting CO-TPD measurement, and the results are shown in Figure 7. It is observed that ZnO/Ag has no signal response, and it is believed that the Ag NPs loaded on ZnO do not provide adsorption sites for CO; on the other hand, the amount of CO adsorbed by the ZnO/Ag@Pd material is much higher than that of ZnO/Pd. The amount of CO adsorbed by ZnO/Ag@Pd is 2.06 times higher than that of the same mass of ZnO/Pd as calculated by the graphic integration of the desorption peaks.

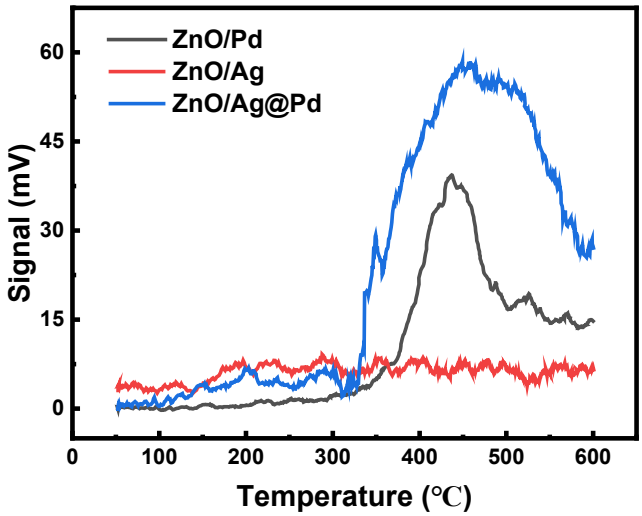

Figure 7. CO-TPD analysis of the ZnO/Pd, ZnO/Ag and ZnO/Ag@Pd.

The particle size of Pd can provide more adsorption sites and catalytic sites on the ZnO surface. When sensing reactions occur, these more catalytic sites can enhance the rate of CH_4 catalytic oxidation reactions, allowing ZnO to exhibit higher response values and to improve its CH_4 sensing performance [15].

Despite the improvement induced by increased Pd dispersities, the effect of interactions between Pd and Ag should be also taken into consideration. Previous studies have proven that the PdAg showed enhanced catalytic effects than compared to Pd or Ag in several systems. Thus, DFT calculation was conducted to study the influence of PdAg bimetallic structures on CH_4 oxidations.

Pd(111) and Ag(111) surfaces were established to study CH_4 adsorption properties on ZnO/Pd and ZnO/Ag according to TEM and XRD results. Ag(111) surfaces doped with Pd atoms (denoted as Ag(111)@Pd surface) were chosen to simulate the structure of Ag@Pd. The adsorption energies of CH_4 on Pd(111), Ag(111) and Ag(111)@Pd surfaces were −0.179, −0.120 and −0.246 eV, respectively, with the order of Ag(111)@Pd > Pd(111) > Ag(111). Furthermore, a differential charge density analysis was performed for the adsorption system with the value of the equivalent surface of 0.001 e/Å^3, and the spatial configurations of the adsorption structure and the differential charge density diagram are shown in Figure 8a–c. The results showed that there was no obvious charge exchange between Ag and CH_4 in Ag(111), while the charge exchange between Pd and CH_4 was more significant in Ag(111)@Pd compared to Pd(111). To further investigate the reason of charge exchange, differential charge density analyses were performed on the blank Ag(111)@Pd for the doped Pd atoms with the value of the equivalent surface of 0.02 e/Å^3. As shown in Figure 8e. It was found that the electron on Pd atoms transferred to Ag after Pd doping, in agreement with the previous XPS analysis.

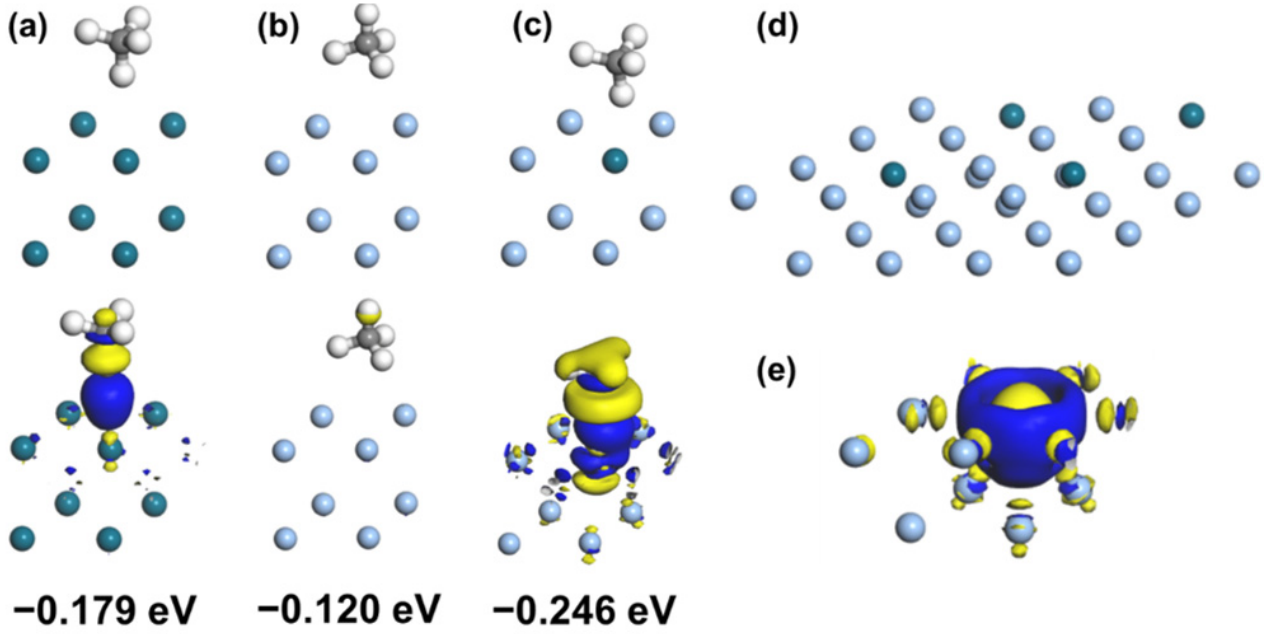

Figure 8. Adsorption energy, spatial configuration and charge density difference of CH_4 molecule on (**a**) Pd(111), (**b**) Ag(111) and (**c**) Ag(111)@Pd surface. (**d**) Relaxed configurations of Ag(111)@Pd surface. (**e**) Charge density difference of the Pd atom on the Ag(111)@Pd surface. Blue indicates electron gain, and yellow indicates electron loss.

From the above results, the mechanism for the CH_4 sensing enhancement by GR method can be concluded in two aspects, as shown in Figure 9. On the one hand, the highly dispersive Pd provided more catalytic sites for CH_4 oxidation with more electrons transferring to ZnO. On the other hand, the bimetallic Ag@Pd structure results in the transfer of electrons from Pd to Ag which makes Pd more positively charged, leading to the stronger adsorption of CH_4 on Pd. Therefore, both effects synergistically contributed to the enhanced CH_4 sensing performance of ZnO/Ag@Pd.

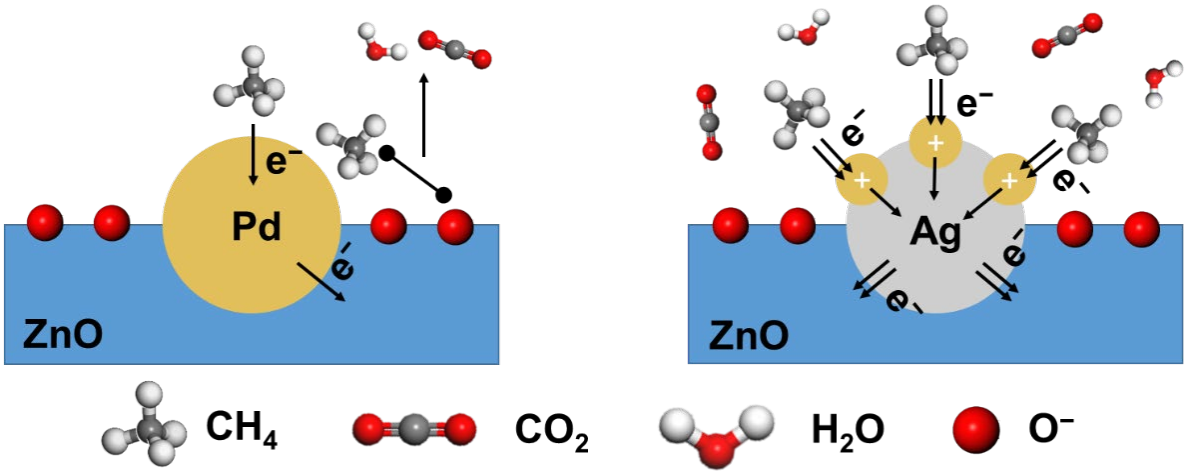

Figure 9. The mechanism for the enhanced sensing performance of CH_4 by the Ag@Pd structure.

4. Conclusions

In this study, the CH_4 sensing performance of ZnO/Pd was investigated, and it was demonstrated that the effect of Pd improving the CH_4 sensing performance has a positive correlation with the dispersity of Pd NPs. Based on this, a highly dispersive loading of Pd on the ZnO surface was achieved by using galvanic replacements using Ag as the sacrificial template. The size of Pd NPs was reduced from 2–4 nm to 1–2 nm with the amount of Pd reduced from 1.35 wt% to 0.23 wt%, while the response of ZnO/Ag@Pd to 500 ppm CH_4 at 230 °C increased from 27.1% to 32.6%. The enhanced performance was attributed to two aspects: The GR method significantly improved the dispersity of Pd NPs which provide more catalytic sites for CH_4 oxidation; Ag@Pd structure by the GR method brought positively charged Pd due to the transfer of electrons from Pd to Ag, which strengthened the adsorption of CH_4. This study provides a strategy for lowering the cost of MOS CH_4 sensors using Pd as a promoter and by reducing the amount of Pd while improving sensing performances, which may provide insights on the reduction in fabrication costs in MOS sensing systems using other noble metals.

Author Contributions: Conceptualization, R.C. and S.L.; methodology, R.C. and S.L.; software, R.C. and Y.Y.; validation, R.C.; formal analysis, R.C.; investigation, R.C.; resources, L.X.; data curation, R.C.; writing—original draft preparation, R.C.; writing—review and editing, S.L., D.X. and L.X.; supervision, D.X. and L.X.; project administration, L.X.; funding acquisition, L.X. All authors have read and agreed to the published version of the manuscript.

Funding: This study was supported by the National Natural Science Foundation of China (grant number 21978153) and the National Key Research and Development Program (grant number 2019YFC1905803).

Institutional Review Board Statement: Not applicable.

Informed Consent Statement: Not applicable.

Data Availability Statement: Not applicable.

Conflicts of Interest: The authors declare no conflict of interest.

References

1. Wang, T.; Zhou, Y.; Luo, Z.; Wen, H.; Zhao, J.; Su, B.; Cheng, F.; Deng, J. Flammability limit behavior of methane with the addition of gaseous fuel at various relative humidities. *Process Saf. Environ. Prot.* **2020**, *140*, 178–189. [CrossRef]
2. Muller, S.; Zimina, A.; Steininger, R.; Flessau, S.; Osswald, J.; Grunwaldt, J.D. High Stability of Rh Oxide-Based Thermoresistive Catalytic Combustion Sensors Proven by Operando X-ray Absorption Spectroscopy and X-ray Diffraction. *ACS Sens.* **2020**, *5*, 2486–2496. [CrossRef]
3. Simion, C.E.; Florea, O.G.; Florea, M.; Neaţu, F.; Neaţu, Ş.; Trandafir, M.M.; Stănoiu, A. CeO_2:Mn_3O_4 Catalytic Micro-Converters Tuned for CH_4 Detection Based on Catalytic Combustion under Real Operating Conditions. *Materials* **2020**, *13*, 2196. [CrossRef]

4. Wang, Y.; Tong, M.M.; Zhang, D.; Gao, Z. Improving the Performance of Catalytic Combustion Type Methane Gas Sensors Using Nanostructure Elements Doped with Rare Earth Cocatalysts. *Sensors* **2011**, *11*, 19–31. [CrossRef]
5. Krishna, K.G.; Parne, S.; Pothukanuri, N.; Kathirvelu, V.; Gandi, S.; Joshi, D. Nanostructured metal oxide semiconductor-based gas sensors: A comprehensive review. *Sens. Actuators A Phys.* **2022**, *341*, 113578. [CrossRef]
6. Ji, H.; Zeng, W.; Li, Y. Gas sensing mechanisms of metal oxide semiconductors: A focus review. *Nanoscale* **2019**, *11*, 22664–22684. [CrossRef] [PubMed]
7. Dey, A. Semiconductor metal oxide gas sensors: A review. *Mater. Sci. Eng. B* **2018**, *229*, 206–217. [CrossRef]
8. Kim, H.-J.; Lee, J.-H. Highly sensitive and selective gas sensors using p-type oxide semiconductors: Overview. *Sens. Actuators B Chem.* **2014**, *192*, 607–627. [CrossRef]
9. Yang, B.; Zhang, Z.; Tian, C.; Yuan, W.; Hua, Z.; Fan, S.; Wu, Y.; Tian, X. Selective detection of methane by HZSM-5 zeolite/Pd-SnO_2 gas sensors. *Sens. Actuators B Chem.* **2020**, *321*, 128567. [CrossRef]
10. Chen, R.; Wang, J.; Luo, S.; Xiang, L.; Li, W.; Xie, D. Unraveling photoexcited electron transfer pathway of oxygen vacancy-enriched ZnO/Pd hybrid toward visible light-enhanced methane detection at a relatively low temperature. *Appl. Catal. B Environ.* **2020**, *264*, 118554. [CrossRef]
11. Tshabalala, Z.P.; Swart, H.C.; Motaung, D.E. Fabrication of TiO_2 nanofibers based sensors for enhanced CH_4 performance induced by notable surface area and acid treatment. *Vacuum* **2021**, *187*, 110102. [CrossRef]
12. Tan, Y.; Lei, Y. Atomic layer deposition of Rh nanoparticles on WO_3 thin film for CH_4 gas sensing with enhanced detection characteristics. *Ceram. Int.* **2020**, *46*, 9936–9942. [CrossRef]
13. Rong, Q.; Xiao, B.; Zeng, J.; Yu, R.; Zi, B.; Zhang, G.; Zhu, Z.; Zhang, J.; Wu, J.; Liu, Q. Pt Single Atom-Induced Activation Energy and Adsorption Enhancement for an Ultrasensitive ppb-Level Methanol Gas Sensor. *ACS Sens.* **2022**, *7*, 199–206. [CrossRef]
14. Wang, Y.; Cui, Y.; Meng, X.; Zhang, Z.; Cao, J. A gas sensor based on Ag-modified ZnO flower-like microspheres: Temperature-modulated dual selectivity to CO and CH_4. *Surf. Interfaces* **2021**, *24*, 101110. [CrossRef]
15. Wang, Y.; Meng, X.; Yao, M.; Sun, G.; Zhang, Z. Enhanced CH_4 sensing properties of Pd modified ZnO nanosheets. *Ceram. Int.* **2019**, *45*, 13150–13157. [CrossRef]
16. Yu, S.; Zhang, H.; Chen, C.; Lin, C. Investigation of humidity sensor based on Au modified ZnO nanosheets via hydrothermal method and first principle. *Sens. Actuators B Chem.* **2019**, *287*, 526–534. [CrossRef]
17. Luo, S.; Zeng, Z.; Zeng, G.; Liu, Z.; Xiao, R.; Chen, M.; Tang, L.; Tang, W.; Lai, C.; Cheng, M.; et al. Metal Organic Frameworks as Robust Host of Palladium Nanoparticles in Heterogeneous Catalysis: Synthesis, Application, and Prospect. *ACS Appl. Mater. Interfaces* **2019**, *11*, 32579–32598. [CrossRef]
18. Sun, J.; Zhang, J.; Fu, H.; Wan, H.; Wan, Y.; Qu, X.; Xu, Z.; Yin, D.; Zheng, S. Enhanced catalytic hydrogenation reduction of bromate on Pd catalyst supported on CeO_2 modified SBA-15 prepared by strong electrostatic adsorption. *Appl. Catal. B Environ.* **2018**, *229*, 32–40. [CrossRef]
19. da Silva, A.G.M.; Rodrigues, T.S.; Haigh, S.J.; Camargo, P.H.C. Galvanic replacement reaction: Recent developments for engineering metal nanostructures towards catalytic applications. *Chem. Commun. (Camb.)* **2017**, *53*, 7135–7148. [CrossRef]
20. Richard-Daniel, J.; Boudreau, D. Enhancing Galvanic Replacement in Plasmonic Hollow Nanoparticles: Understanding the Role of the Speciation of Metal Ion Precursors. *ChemNanoMat* **2020**, *6*, 907–915. [CrossRef]
21. Guo, S.; Zhang, G.; Han, Z.-K.; Zhang, S.; Sarker, D.; Xu, W.W.; Pan, X.; Li, G.; Baiker, A. Synergistic Effects of Ternary PdO–CeO_2–OMS-2 Catalyst Afford High Catalytic Performance and Stability in the Reduction of NO with CO. *ACS Appl. Mater. Interfaces* **2021**, *13*, 622–630. [CrossRef]
22. Zhang, Y.; Yang, X.; Zhou, Y.; Li, G.; Li, Z.; Liu, C.; Bao, M.; Shen, W. Selective hydrogenation of the C=C bond in α,β-unsaturated aldehydes and ketones over ultra-small Pd–Au clusters. *Nanoscale* **2016**, *8*, 18626–18629. [CrossRef] [PubMed]
23. Luo, S.; Chen, R.; Wang, J.; Xie, D.; Xiang, L. Designed synthesis of ZnO/Pd@ZIF-8 hybrid structure for highly sensitive and selective detection of methane in the presence of NO_2. *Sens. Actuators B Chem.* **2021**, *344*, 130220. [CrossRef]
24. Chen, R.S.; Wang, J.; Xia, Y.; Xiang, L. Near infrared light enhanced room-temperature NO_2 gas sensing by hierarchical ZnO nanorods functionalized with PbS quantum dots. *Sens. Actuators B Chem.* **2018**, *255*, 2538–2545. [CrossRef]
25. Delley, B. An All-Electron Numerical-Method for Solving the Local Density Functional for Polyatomic-Molecules. *J. Chem. Phys.* **1990**, *92*, 508–517. [CrossRef]
26. Delley, B. From molecules to solids with the $DMol^3$ approach. *J. Chem. Phys.* **2000**, *113*, 7756–7764. [CrossRef]
27. Perdew, J.P.; Burke, K.; Ernzerhof, M. Generalized gradient approximation made simple. *Phys. Rev. Lett.* **1996**, *77*, 3865–3868. [CrossRef]
28. Wang, H.; Qiao, X.; Chen, J.; Wang, X.; Ding, S. Mechanisms of PVP in the preparation of silver nanoparticles. *Mater. Chem. Phys.* **2005**, *94*, 449–453. [CrossRef]